Krogager Decomposition and Pseudo-Zernike Moments for Polarimetric Distributed ATR

Domenico Gaglione*, Carmine Clemente*, Luca Pallotta†,
Ian Proudler‡, Antonio De Maio§, and John J. Soraghan*
*University of Strathclyde, CESIP, EEE, 204, George Street, G1 1XW, Glasgow, UK
E-mail: domenico.gaglione@strath.ac.uk, carmine.clemente@strath.ac.uk, j.soraghan@strath.ac.uk
† CNIT c/o udr Università "Federico II", via Claudio 21, I-80125 Napoli, Italy
E-mail: luca.pallotta@unina.it
‡ School of Electronic, Electrical and Systems Engineering, Loughborough University, Leicestershire, UK
E-mail: i.k.proudler@lboro.ac.uk
§Università degli Studi di Napoli "Federico II", DIETI, via Claudio 21, I-80125 Napoli, Italy
E-mail: ademaio@unina.it

***Abstract*—Automatic Target Recognition (ATR) is one of the most challenging areas of the modern radar signal processing field. In this paper a recognition algorithm for full-polarimetric SAR images, that is robust with respect to rotations and target roll, is presented. It is based on the use of the pseudo-Zernike moments and the Krogager decomposition components, and exploits multiple sources of information such as polarization and spatial diversity. The effectiveness of the proposed approach has been demonstrated with real full polarimetric SAR data.**

I. Introduction

Automatic Target Recognition (ATR) is one of the main application of modern radar systems. Although it can find applications in non-military problems, ATR is an essential requirement in battlefield scenarios, where the correct identification of a target must be guaranteed with high degree of confidence. In this context, multiple sources of information are often available (i.e. spatial, temporal, frequency, waveform and polarization diversities) and they can be potentially combined leading to an improvement of the performance.

ATR generally refers to two different tasks: detection and recognition. The former deals with the problem of locating a target, while the latter deals with the classification of a target by means of the exploitation of a priori knowledge (i.e. a database). In [1] we have presented an algorithm for target classification from multi-sensor full-polarimetric SAR data, which exploits both the diversity offered by the use of different sensors, and the different scattering responses of an object in each polarimetric channel. More specifically, the term multi-sensor has been used to indicate that images of the scene acquired from different view points are used to perform the classification; however, the developed framework can also be used with images acquired, for example, with a multi-frequency sensor. The algorithm takes as input the four polarimetric components of the object under test, from which some discriminating features based on the pseudo-Zernike (PZ) moments are extracted and used to recognize the target by using a classifier. If multiple views are available, they are processed separately and then the decisions of all the classifiers are combined, leading to an estimate of the class to which the target belongs. The effectiveness of this approach was demonstrated in [2].

The effectiveness of the use of PZ based features for radar ATR application was also successfully demonstrated in [3], where novel features were developed for micro-Doppler classification.

In this paper a novel extension of the algorithm presented in [1] is proposed. The Krogager polarimetric decomposition [4] is applied to the full-polarimetric image, and then, according to a fusion rule, the classification is performed by exploiting both the polarimetric and the Krogager components of the target.

The remainder of the paper is organised as follows. Section II and Section III introduce the Krogager polarimetric decomposition and the PZ moments, respectively. The proposed algorithm is presented in Section IV. Relative performance evaluation results using the GOTCHA dataset [5] are included in Section V. Section VI concludes the paper.

II. Krogager Decomposition

The physical interpretation of a SAR image, in particular a full-polarimetric SAR image, can often be extremely difficult. The objective of a polarimetric decomposition is to express the scattering matrix (coherent decomposition), or the covariance matrix if a second order description is needed (incoherent decomposition), as a combination of canonical objects which present an easier physical interpretation.

Let $\mathbf{S}(x,y)$ denote a 2-by-2 scattering matrix. A coherent polarimetric decomposition can be expressed as

$$\mathbf{S}(x,y) = \sum_{m=1}^{M} c_m \mathbf{S}_m(x,y), \tag{1}$$

where $\mathbf{S}_m(x,y)$ is the response of the m-th canonical object, c_m indicates the weight of $\mathbf{S}_m(x,y)$ in the combination leading to $\mathbf{S}(x,y)$, M is the number of components, x and y are the spatial coordinates. The Krogager polarimetric decomposition is defined by means of the circular polarization scattering matrix $\mathbf{S}_{(R,L)}(x,y)$, where the letter R indicates the right-handed circular component and L represents the left-handed circular component. In a monostatic radar, such as SAR, the scattering matrix is symmetric, therefore the $\mathbf{S}_{(R,L)}(x,y)$ components can be expressed in terms of the linear polarization

978-1-4799-5294-6/14/$31.00 ©2014 IEEE

components as follows [6]

$$S_{RR}(x,y) = \frac{S_{HH}(x,y) - S_{VV}(x,y)}{2} + iS_{HV}(x,y), \quad (2)$$

$$S_{LL}(x,y) = \frac{S_{HH}(x,y) - S_{VV}(x,y)}{2} - iS_{HV}(x,y), \quad (3)$$

$$S_{RL}(x,y) = S_{LR}(x,y) = \frac{S_{HH}(x,y) + S_{VV}(x,y)}{2}, \quad (4)$$

where i is the imaginary unit. From [7] and neglecting the (x,y) dependence in order to simplify the equations, the Krogager polarimetric decomposition is defined as

$$\mathbf{S}_{(R,L)} = \begin{bmatrix} S_{RR} & S_{RL} \\ S_{LR} & S_{LL} \end{bmatrix} = e^{i\phi}\left\{ k_s e^{i\phi_s} \begin{bmatrix} 0 & i \\ i & 0 \end{bmatrix} + k_d \begin{bmatrix} e^{i2\eta} & 0 \\ 0 & -e^{-i2\eta} \end{bmatrix} + k_h \begin{bmatrix} e^{i2\eta} & 0 \\ 0 & 0 \end{bmatrix} \right\}, \quad (5)$$

where k_s, k_d and k_h are real-valued quantities which can be interpreted as scattering coefficients from a sphere, a diplane and a helix, respectively. Moreover, ϕ is the absolute phase term which depends on the distance between the target and the sensor, ϕ_s represents the displacement of the sphere with respect to the diplane and the helix components, and η is their orientation angle. The scattering coefficients k_s, k_d and k_h may be computed from the circular polarization scattering components [8] as follows:

$$k_s = |S_{RL}|, \quad (6)$$

$$k_d = \min\left(|S_{RR}|, |S_{LL}|\right), \quad (7)$$

$$k_h = \mathrm{abs}(|S_{RR}| - |S_{LL}|), \quad (8)$$

where the symbol $|\cdot|$ indicates the modulus of a complex quantity and $\mathrm{abs}(\cdot)$ stands for absolute value.

In several earlier studies, the Krogager decomposition has been shown to be the most suitable, among other coherent polarimetric decompositions, in dividing man-made targets from natural targets [8]-[9], however it is not capable of distinguish between different man-made targets [10]. Furthermore, in [11] is shown that k_s, k_d and k_h are roll-invariant. Consequently they do not depend on the orientation of the target in roll (meaning invariance with respect to observation from platforms with different incidence angles).

III. Pseudo-Zernike Moments

The PZ moments are used in signal processing for their low computational complexity and specific properties, such as invariance with respect to translation and rotation.

Let $f(x,y) \in \mathbb{R}$, with $f(x,y) \geq 0$; then the complex-valued PZ moment of $f(x,y)$ is defined as its projection on the PZ polynomial $W_{n,l}(\rho,\theta)$ of degree $n \geq |l|$

$$\psi_{n,l} = \frac{n+1}{\pi} \int_0^{2\pi} \int_0^1 W^*_{n,l}(\rho,\theta) f(\rho\cos\theta, \rho\sin\theta) \rho \mathrm{d}\rho \mathrm{d}\theta, \quad (9)$$

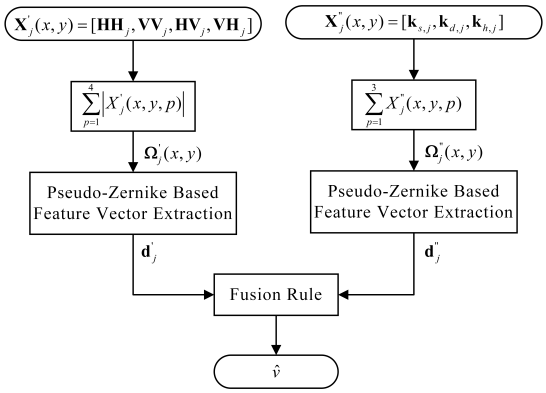

Fig. 1. Block diagram of the proposed algorithm.

where the symbol $(\cdot)^*$ indicates the complex conjugate operator, $\rho = \sqrt{x^2+y^2}$, $\theta = \tan^{-1}(y/x)$ and

$$W_{n,l}(\rho,\theta) = S_{n,l}(\rho)e^{il\theta} = \sum_{m=0}^{n-|l|} \frac{\rho^{n-m}(-1)^m(2n+1-m)!}{m!(n+|l|+1-m)!(n-|l|-m)!} e^{il\theta}. \quad (10)$$

Some important properties of the PZ polynomials are provided in [12]. It is demonstrated that the functions $W_{n,l}(\rho,\theta)$ form a complete basis and satisfy the orthogonality relation on the unit disc (i.e for $\rho \leq 1$), that is

$$\int_0^{2\pi} \int_0^1 W^*_{n,l}(\rho,\theta) W_{m,k}(\rho,\theta) \rho \mathrm{d}\rho \mathrm{d}\theta = \frac{\pi}{n+1} \delta_{nm}\delta_{lk}, \quad (11)$$

where $\delta_{nm} = 1$ if $n = m$ and 0 otherwise. Hence, since the number of orthogonal polynomials is $(n+1)^2$ (once n is given), this is also the number of independent PZ moments. Another important characteristic relates to the modulus of the polynomial in (10), which is rotational invariant. This makes also the modulus of the PZ moments rotational invariant.

IV. Proposed Algorithm

The proposed approach is described in detail in the next two sub-sections; the former presents the feature extraction procedure, while the latter introduces the fusion rule.

A. Feature Extraction

The algorithm is based on the use of both the full-polarimetric image and the Krogager components of the target. As illustrated in Fig. 1, $\mathbf{X}'_j(x,y)$ and $\mathbf{X}''_j(x,y)$ are the vectors whose elements are the four polarimetric components and the three Krogager components of the target, respectively, that is

$$\mathbf{X}'_j(x,y) = \left[\mathbf{HH}_j(x,y), \mathbf{VV}_j(x,y), \mathbf{HV}_j(x,y), \mathbf{VH}_j(x,y)\right] \in \mathbb{C}^{B\times Q\times 4} \quad (12)$$

and

$$\mathbf{X}''_j(x,y) = \left[\mathbf{k}_{s,j}(x,y), \mathbf{k}_{d,j}(x,y), \mathbf{k}_{h,j}(x,y)\right] \in \mathbb{R}^{B\times Q\times 3}, \quad (13)$$

where $B \times Q$ is the dimension of the image that includes the target and the subscripts j indicates that the image comes from the j-th sensor. More specifically, the matrices $\mathbf{k}_s$, $\mathbf{k}_d$ and $\mathbf{k}_h$ contain, pixel-by-pixel, the Krogager components k_s, k_d and

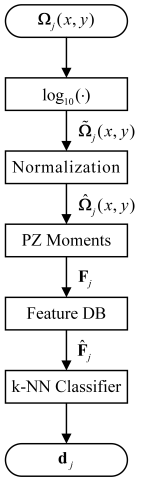

Fig. 2. Pseudo-Zernike based feature vector extraction block.

k_h, which emphasise the single bounce, the double bounce and the volumetric scattering of the scene; thus, from them is possible to extract PZ based features which are different from those extracted from the full-polarimetric image.

The PZ based feature vector extraction block is shown in Fig. 2. The image $\mathbf{\Omega}_j(x,y)$, which is the result of the sum of either the magnitude of the polarimetric components ($\mathbf{\Omega}_j^{'}(x,y)$) or the Krogager components ($\mathbf{\Omega}_j^{''}(x,y)$), is scaled and normalized as follows

$$\tilde{\mathbf{\Omega}}_j(x,y) = \log_{10}(\mathbf{\Omega}_j(x,y)), \tag{14}$$

$$\overline{\mathbf{\Omega}}_j(x,y) = \tilde{\mathbf{\Omega}}_j(x,y) - \min \tilde{\mathbf{\Omega}}_j(x,y), \tag{15}$$

$$\hat{\mathbf{\Omega}}_j(x,y) = \overline{\mathbf{\Omega}}_j(x,y) / \max \overline{\mathbf{\Omega}}_j(x,y). \tag{16}$$

The logarithm is performed to reduce the dynamic range of the image, while (15)-(16) restrict it into the range $[0,1]$ in order to obtain features that are independent of different intensity levels.

Since the polynomials in (10) are defined on the unit disc, to avoid information loss the support of $\hat{\mathbf{\Omega}}_j(x,y)$ is scaled before its PZ moments are computed. The output of the PZ Moments sub-block (Fig. 2) is a vector, $\mathbf{F}_j$, whose length is $(n+1)^2$ and whose elements are the modulus of the PZ moments up to the order n, that is

$$\begin{aligned}\mathbf{F}_j = \big[&|\psi_{0,0}|, \ldots, |\psi_{n,-n}|, |\psi_{n,-(n-1)}|, \ldots, \\ &|\psi_{n,(n-1)}|, |\psi_{n,n}|\big].\end{aligned} \tag{17}$$

From (17), the feature vector, $\hat{\mathbf{F}}_j$, is then computed by using the following linear rescaling

$$\hat{\mathbf{F}}_j = \frac{\mathbf{F}_j - \mu_{\mathbf{F}_j}}{\sigma_{\mathbf{F}_j}}, \tag{18}$$

where $\mu_{\mathbf{F}_j}$ and $\sigma_{\mathbf{F}_j}$ are the mean and the standard deviation of the vector $\mathbf{F}_j$, respectively. Note that, since the PZ polynomials in (10) depend on the image size $B \times Q$ only, they can be pre-computed and stored in a look up table, and then used for the feature extraction from different targets.

The last step in Fig. 2 is the classification, carried out by using a k-Nearest Neighbour (k-NN) classifier. It returns a score vector $\mathbf{d}_j \in \mathbb{R}^V$, where V is the number of possible classes, whose elements are the occurrences (normalized to k) of each class among the k nearest neighbours to $\hat{\mathbf{F}}_j$.

B. Fusion Rule

Let J be the number of sensors, or full-polarimetric images, available to classify the target; this means that $2J$ score vectors are input to the fusion rule block in Fig. 1, J for each branch, that is

$$\mathbf{d}_j^{'} \qquad j = 1, \ldots, J, \tag{19}$$

$$\mathbf{d}_j^{''} \qquad j = 1, \ldots, J. \tag{20}$$

The adopted fusion rule consists of adding up these vectors and deciding for the class which presents the largest total score. Thus

$$\boldsymbol{\lambda} = \sum_{j=1}^{J} \mathbf{d}_j^{'} + \sum_{j=1}^{J} \mathbf{d}_j^{''}, \tag{21}$$

where $\boldsymbol{\lambda} = [\lambda_1, \lambda_2, \ldots \lambda_V]$, and then the estimated class is selected as

$$\hat{v} = \begin{cases} \underset{v}{\operatorname{argmax}}\, \boldsymbol{\lambda} & \text{if } \exists!(\max \boldsymbol{\lambda}) > T \\ \textit{unknown} & \text{otherwise} \end{cases} \tag{22}$$

The thresholding is performed because the largest value of $\boldsymbol{\lambda}$ may not be large enough to consider the classification reliable, in which case the target under test is declared *unknown*, which means that it cannot be classified. Note that the *unknown* declaration also occurs when the largest value of $\boldsymbol{\lambda}$ has more than one occurrence.

V. Performance Analysis

In this section, the algorithm is tested using the GOTCHA dataset [5], which is a collection of real full-polarimetric circular SAR images acquired by an airborne X-band sensor (carrier frequency 9.6 GHz) with a 640 MHz bandwidth at 8 different elevation angles; the set consists of 2880 full-polarimetric images, 360 for each pass, of several civilian vehicles and calibration targets.

In the following sub-sections, the training and the test sets are described, and the results of the analysis are shown.

A. Training Set and Test Set

For our purpose, the full synthetic aperture (360°) has been divided into 90 sub-apertures of 4° in azimuth each, in order to have approximately equal range-azimuth resolution cells of 23 cm; thus, the set used is made up of 720 full-polarimetric images for each of the 9 commercial vehicles considered as target, which are shown in Fig. 3(a). From the entire scene (Fig. 3(b)), equal-sized sub-images (51×46 pixels) containing each vehicle are selected; this means that in (12)-(13) $B = 51$ and $Q = 46$.

Six different analyses are presented, as combination of two configurations for the training set and three configurations for the test set. The training set is formed by images coming from the lowest altitude pass; either 10 or 30 images for each vehicles are used to train the classifiers, selected each 36° or 12° in azimuth. The test set is formed by all but the images used for the training. Three configurations are considered: in the first scenario (Fig. 4(a)), one image is used in order to classify the target, which is equivalent to having $J = 1$; in the other two scenarios, shown in Fig. 4(b) and Fig. 4(c), 2 and

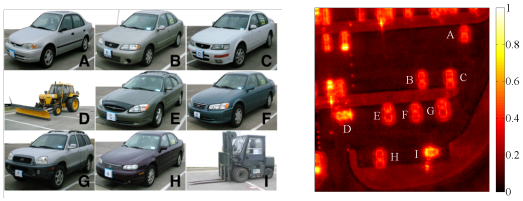

(a) (b)

Fig. 3. GOTCHA Dataset: (a) images of the vehicles used as targets; (b) full-azimuth and full-polarimetric magnitude SAR image of the area of interest containing the 9 vehicles.

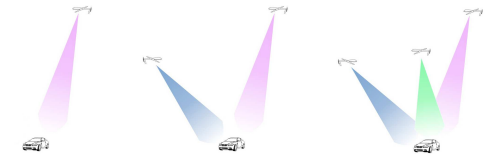

(a) (b) (c)

Fig. 4. Test configurations: (a) 1, (b) 2 and (c) 3 sensors cases.

TABLE I. THRESHOLDS.

	1 Sensor	2 Sensors	3 Sensors
IA	1/3	2/3	4/3
KA	1/3	2/3	4/3
IIK	2/3	4/3	8/3

3 images are used ($J = 2$ and $J = 3$) to show the benefits of the multi-sensor framework.

The results are presented in terms of percentage of correct classification, defined as the number of targets correctly classified normalized to the total number of targets under test and expressed as percentage; note that, besides the targets classes A to I, a tenth output class is considered, which contains the objects which have been declared as *unknowns* (the chosen thresholds T, defined in (22), are summarised in Table I). For the case of 1 sensor, all the available images are used for the testing, that is 710 images for each target if the training is performed with 10 images, 690 images for the 30 training images case. For the case of 2 and 3 sensors, 71000 or 69000 couples and triples are chosen randomly, depending on the training configurations; for this reason, the standard deviation of the correct classification rate, σ, is also computed. Moreover, the analysis is performed for different values of the order of the PZ polynomial and using a 3-NN classifier; this value of k resulted to be the most effective in [2].

B. Results

In this sub-section, the performance of the proposed algorithm, which will be labelled as Integrated Intensity-Krogager (IIK) approach, is shown and compared with the performance of the Intensity Approach (IA), proposed in [1], and of the Krogager Approach (KA); the latter consists of classifying the target by using only the vector $\mathbf{X}_j''(x, y)$.

In Fig. 5, the percentage of correct classification and the percentage of unknowns, which is the number of targets declared as unknown normalized to the total number of targets under test and expressed as percentage, are shown for the case $J = 1$. As expected, the correct classification rate increases as the order of the PZ moments increases, while the unknowns rate has an opposite trend. The IIK approach shows better performance both when 10 images are used for the training

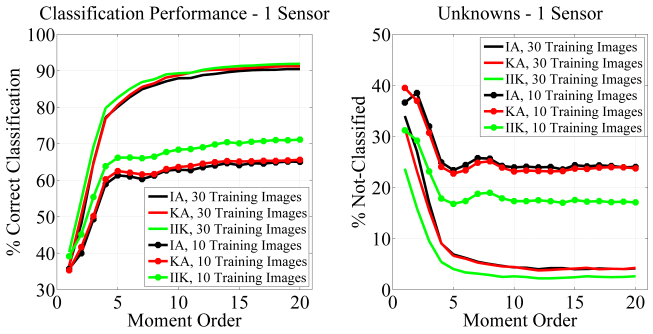

Fig. 5. Results 1 sensor: percentage of correct classification (left) and percentage of unknowns (right).

and when 30 images are used. Tables II and III summarise the performance improvement of the IIK compared to the IA. From the tables it is seen that in the first case the average increase in terms of percentage of correct classification is 5.51%, while the average decrease in terms of percentage of unknowns is 6.95%; in the second case, the improvement of the ratio of correct classification is 2.16% in average, while the average decrease of the unknowns rate is 3.18%.

In Fig. 6 and Fig. 7, results for the cases $J = 2$ and $J = 3$

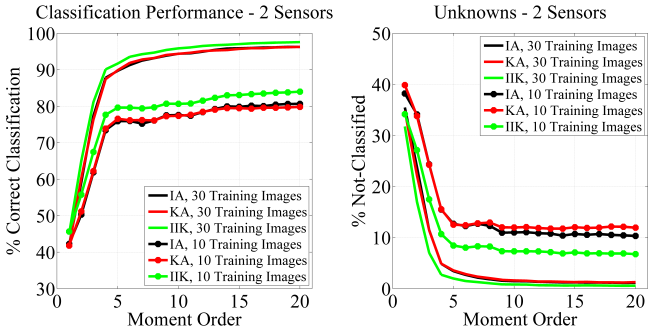

Fig. 6. Results 2 sensors: percentage of correct classification (left) and percentage of unknowns (right).

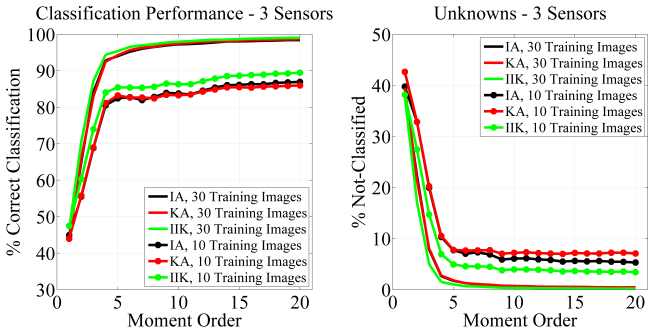

Fig. 7. Results 3 sensors: percentage of correct classification (left) and percentage of unknowns (right).

are shown, respectively. From these figures and the second and the third columns in Table II and III, it is clear that the exploitation of the spatial diversity leads to better performance compared to the case $J = 1$. Moreover, as highlighted above, the IIK approach presents improvements both in terms of percentage of correct classification and in terms of percentage of unknowns. Table IV shows the confusion matrix for the IIK approach. In this case $J = 3$, 10 training images are used and PZ moments order is equal to 10. It can be seen how the

TABLE II. IA - IIK COMPARISON: AVERAGE INCREASES OF THE CORRECT CLASSIFICATION PERCENTAGE.

	1 Sensor	2 Sensors	3 Sensors
10 Training Images	5.51%	3.62%	2.93%
30 Training Images	2.16%	1.92%	1.24%

TABLE III. IA - IIK COMPARISON: AVERAGE DECREASES OF THE UNKNOWNS PERCENTAGE.

	1 Sensor	2 Sensors	3 Sensors
10 Training Images	6.95%	4.16%	2.51%
30 Training Images	3.18%	1.44%	0.74%

TABLE IV. CONFUSION MATRIX: 3 SENSORS CASE, 10 TRAINING IMAGES, PSEUDO-ZERNIKE MOMENTS ORDER 10.

	A	B	C	D	E	F	G	H	I	Unk
A	697	0	0	0	3	0	0	1	1	8
B	0	654	0	0	0	0	37	0	0	19
C	0	0	390	0	0	11	0	253	0	56
D	0	0	0	650	52	0	0	0	0	8
E	0	0	0	8	690	0	0	0	0	12
F	0	0	24	0	0	653	0	9	0	24
G	0	91	0	3	0	0	480	1	0	135
H	0	0	140	0	0	17	0	531	0	22
I	0	0	0	0	0	0	0	0	710	0

TABLE V. CONFIDENCE INTERVALS $1 \times \sigma$.

	2 Sensors	3 Sensors
10 Training Images	0.74%	0.82%
30 Training Images	0.67%	0.74%

target G has the higher percentage of unknowns (about 19.0%) and is confused with B, while C is confused with H, and vice versa, in the 35.63% and 19.72% of the cases, respectively. As mentioned above, for the $J = 2$ and $J = 3$ cases the standard deviation has also been computed; the results, summarised in Table V, show that the $1 \times \sigma$ confidence intervals are always less then 1%.

Hence, the proposed approach presents better performance for all the configurations in which it has been tested. In particular, from Table II and Table III, it is noted that the best improvements are achieved in the case in which 10 images for the training are used; this means that in order to reach the same performance, the IIK approach requires less a priori information compared to the IA, which implies less cost, since the acquisition of a targets database is often expensive and time consuming. In addition to the general increase of the percentage of correct classification, the decrease of the unknowns rate makes the IIK approach even more reliable than the IA method. Moreover, the PZ moments properties of translation and rotation independence, combined with the roll invariant characteristic of the Krogager decomposition, makes the algorithm robust with respect to both the target orientation in the image plane and the acquisition elevation angle. Note that these improvements are obtained only at cost of a small computational increase, since no additional information is required as input of the algorithm with respect to the IA.

VI. CONCLUSION

In this paper a novel ATR algorithm was presented, which uses one or more full-polarimetric SAR images of a target to perform the classification. Unlike the IA presented in [1], the decision is based on the use of both the four polarimetric components and the three Krogager components of the target. The framework has been tested by using a full-polarimetric SAR images set of several civilian vehicles; the results show that the proposed approach achieves better performance than the approach presented in [1] in terms of percentage of correct classification and percentage of unknowns, only at cost of a slight increase in computational complexity. Moreover, the properties of rotationally invariant and roll invariant of the PZ moments and Krogager components, respectively, make the algorithm robust with respect to the orientation of the target and to the acquisition elevation angle. Notice that the framework can also find application in a real-time scenario, in which several sensors are involved. In such a case, the information that each sensor has to send to the fusion centre, only regards its score vectors $\mathbf{d}_j^{'}$ and $\mathbf{d}_j^{''}$, and the position of the target, with low complexity and bandwidth requirements. Future work will deal with the development of a weighted fusion rule and the computation of optimal weights on varying the SAR depression angle.

ACKNOWLEDGMENT

This work was supported by the Engineering and Physical Sciences Research Council (EPSRC) Grant number EP/K014307/1 and the MOD University Defence Research Collaboration in Signal Processing, and University of Naples "Federico II".

REFERENCES

[1] C. Clemente, L. Pallotta, I. Proudler, A. De Maio, J.J. Soraghan, and A. Farina, "Multi-Sensor Full-Polarimetric SAR Automatic Target Recognition Using Pseudo-Zernike Moments," in *International Radar Conference 2014*, Lille, France, Oct. 13–17, 2014.

[2] C. Clemente, L. Pallotta, I. Proudler, A. De Maio, J.J. Soraghan, and A. Farina, "Pseudo-Zernike Based Multi-Pass Automatic Target Recognition From Multi-Channel SAR," *CoRR*, vol. abs/1404.1682, 2014.

[3] L. Pallotta, C. Clemente, A. De Maio, J.J. Soraghan, and A. Farina, "Pseudo-Zernike Moments Based Radar Micro-Doppler Classification," in *IEEE Radar Conference*, Cincinnati, USA, May 19–23, 2014.

[4] E. Krogager, "New decomposition of the radar target scattering matrix," *Electronics Letters*, vol. 26, no. 18, pp. 1525–1527, 1990.

[5] E. Ertin, C.D. Austin, S. Sharma, R.L. Moses, and L.C. Potter, "GOTCHA experience report: three-dimensional SAR imaging with complete circular apertures," 2007, vol. 6568, pp. 656802–656802–12.

[6] M.A. Richards, J. Scheer, and W.A. Holm, *Principles of Modern Radar: Basic Principles*, SciTech Pub., 2010.

[7] M. Hellmann and E. Krogager, "Comparison of Decompositions for pol-SAR Image Interpretation," in *Geoscience and Remote Sensing Symposium, 2000. Proceedings. IGARSS 2000. IEEE 2000 International*. IEEE, 2000, vol. 3, pp. 1313–1315.

[8] V. Alberga, E. Krogager, M. Chandra, and G. Wanielik, "Potential of coherent decompositions in SAR polarimetry and interferometry," in *Geoscience and Remote Sensing Symposium, 2004. IGARSS'04. Proceedings. 2004 IEEE International*. IEEE, 2004, vol. 3, pp. 1792–1795.

[9] Q. Wei, C. Jian-Jun, Z. Hong-Zhong, and Z. Feng, "Target Decomposition for Fully Polarimetric Wideband Radar System," in *Signal Processing (ICSP), 2010 IEEE 10th International Conference on*. IEEE, 2010, pp. 2246–2249.

[10] L. Zhang, J. Zhang, B. Zou, and Y. Zhang, "Comparison of Methods for Target Detection and Applications Using Polarimetric SAR Image," *Piers online*, vol. 4, no. 1, pp. 140–145, 2008.

[11] E. Krogager, "Properties of the sphere, diplane, helix (target scattering matrix) decomposition," *Proc. of JIPR-3, Mar. 1995*, 1995.

[12] A.B. Bhatia and E. Wolf, "On the circle polynomials of Zernike and related orthogonal sets," in *Proc. Cambridge Philos. Soc*. Cambridge Univ Press, 1954, vol. 50, pp. 40–48.